

Paper:

Visual Servoing for Underwater Vehicle Using Dual-Eyes Evolutionary Real-Time Pose Tracking

Myo Myint, Kenta Yonemori, Akira Yanou, Khin Nwe Lwin,
Mamoru Minami, and Shintaro Ishiyama

Graduate School of Natural Science and Technology, Okayama University

3-1-1 Tsushima-naka, Kita-ku, Okayama 700-8530, Japan

E-mail: minami-m@cc.okayama-u.ac.jp

[Received December 9, 2015; accepted May 17, 2016]

Recently, a number of researches related to underwater vehicle has been conducted worldwide with the huge demand in different applications. In this paper, we propose visual servoing for underwater vehicle using dual-eyes cameras. A new method of pose estimation scheme that is based on 3D model-based recognition is proposed for real-time pose tracking to be applied in Autonomous Underwater Vehicle (AUV). In this method, we use 3D marker as a passive target that is simple but enough rich of information. 1-step Genetic Algorithm (GA) is utilized in searching process of pose in term of optimization, because of its effectiveness, simplicity and promising performance of recursive evaluation, for real-time pose tracking performance. The proposed system is implemented as software implementation and Remotely Operated Vehicle (ROV) is used as a test-bed. In simulated experiment, the ROV recognizes the target, estimates the relative pose of vehicle with respect to the target and controls the vehicle to be regulated in desired pose. PID control concept is adapted for proper regulation function. Finally, the robustness of the proposed system is verified in the case when there is physical disturbance and in the case when the target object is partially occluded. Experiments are conducted in indoor pool. Experimental results show recognition accuracy and regulating performance with errors kept in centimeter level.

Keywords: visual servoing, stereo camera, genetic algorithm, underwater vehicle, model-based recognition

1. Introduction

Nowadays, visual servoing in which visual information is used to control the robot's motion plays an important role in different domains of application with the rapid progresses in computer vision technology. Generally, visual servoing techniques are divided into two categories; Image-Based Visual Servoing (IBVS) and Position-Based Visual Servoing (PBVS). In IBVS techniques, images from camera are used directly for control of robot. In

PBVS, information of known object are extracted and interpreted from the images and used in controlling of robot in reference space rather than in image space as in IBVS [1–3]. Based on the location of camera, eye-in-hand and eye-to-hand configuration are considered according to the requirement of application. Then, the techniques are differentiated based on the number of cameras; from single to multi cameras. Even though there are some limitations for real-time applications in terms of image-acquisition-quantization accuracy and processing rates, the role of visual information has been expanding rapidly in industry and human society in line with efforts of researchers [4, 5].

Like the land and space systems, a number of researches on underwater vehicle using visual servoing has been conducted worldwide recently [6–24]. Each of them is with different merits and limitations. Most of researches are based on the monocular vision [6, 7]. In [8], vision system using artificial underwater landmarks in order to be able to act autonomously using two cameras was reported. In the contribution of [9], features in plate are extracted and relative pose is estimated using the oriented FAST and rotated BRIEF (ORB) feature extractor. Even though two cameras are equipped in [8, 9], only one of cameras is used to estimate the position and orientation of the target and another camera is for another task. There are some related works using stereo vision for underwater vehicle [10, 11]. In [10], a new approach of position measurement for underwater vehicle-manipulator systems using pan-tilt-slide cameras categorized in IBVS was proposed. Epipolar geometry calculation of target consisting of three LED is realized using slide mechanism. Combining monocular and binocular vision positioning algorithm was introduced in [11], reducing limitation of image matching technique using two cameras. In [11], dead reckoning algorithm was introduced as an aided navigation because of longer computing time for vision based navigation. Geometry calculation for relative position of target consisting of LED is used in both [10, 11]. In contrast, we have developed vision-based underwater vehicle using standalone dual-eyes cameras and 3D marker in PBVS that is passive target for real-time pose tracking as shown in Fig. 1.

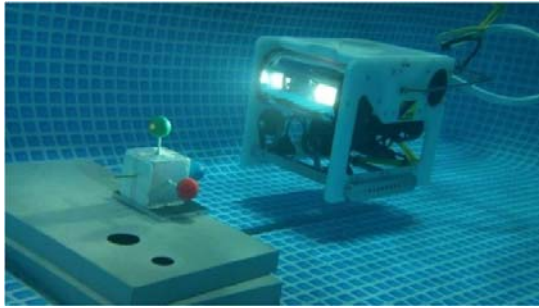


Fig. 1. Underwater vehicle and 3D marker.

In proposed system, the system estimates a relative position and orientation between ROV and target object using 3D model-based matching method utilizing genetic algorithm. We examined regulating relative pose performance that means the robot has to be kept constant in the desired relative pose with respect to the target even though there is disturbance and 3D marker is partially occluded. It is shown experimentally that regulating experiment can be implemented using proposed system, approving its robustness.

The paper is organized as follows: Section 2 presents problem statement of the proposed work. Section 3 describes the proposed system along with the detailed explanation of the system. Experiments to assess the performance of the proposed system are described in Section 4. Experimental results and discussions are presented in Section 5. The final section concludes the paper.

2. Problem Statement

Most of the related works reported for pose estimation are based on features-based method in which man-made features are extracted from images and matched the corresponding features in other images [3, 10]. There are some notable studies on 3D pose estimation and tracking [25–29]. In 3D pose estimation, interpretation such as epipolar geometry using multiple views provides precise pose estimation, especially camera depth measurement. However, these methods demand huge computation load for real-time application and matching between interested features makes the system performance too much dependent especially on corresponding authenticity of points in the images of plural cameras. The wrong points pairs induce 3D pose estimation errors, resulting in corruption of visual servoing closed loop. Therefore, 3D reconstruction techniques are too expensive for accurate pose estimation of the known object. Avoiding these limitations in features-based methods that are based on 2D to 3D reconstruction, pose estimation using 3D model-based matching utilizing GA based on the concept of 3D to 2D projection is utilized in this paper.

Apart from indoor visual servoing environment, real underwater environment provides different kinds of disturbances in terms of physical disturbance to the movement of vehicle due to ocean current and target occlusion

especially when vision-sensor is dominant in navigation sensor unit. Therefore, the robustness of proposed system is verified in regulating performance in the case when there is physical disturbance from different directions of vehicle and in the case when the target is partially occluded.

3. Proposed System

This paper introduces one of solutions for motion control of underwater vehicle using vision-based control. The basic concept of the vision-based control technology is to minimize an error that is represented by difference between image measurement and desired value. In proposed system, desired value is relative pose (position and orientation) of vehicle with respect to target in Cartesian space rather than in image space and image measurements are a set of 3D parameters from which current pose is estimated in real-time.

The main task of this work is to control the underwater vehicle to be regulated in desired pose to the target by means of visual servoing. In this system, the images acquired from the dual-eyes cameras are sent to a PC. Then, the real-time 3D pose estimation of the target object is executed in software implementation of the PC. Finally, based on the error between target value and estimated value, command signals generated from calculating the voltage value gained by P controller for the thrusters are input into ROV in order to keep desired pose. According to effectiveness, 3D model-based matching method is reported for 3D pose estimation for AUV.

3.1. 3D Model-Based Matching Method Using Stereo Vision

Instead of calculation of the absolute position of the vehicle and the target, the relative pose of the vehicle with respect to the known target is estimated using 3D model-based recognition. In this method, knowing the information of the 3D marker and desired relative pose to the underwater vehicle, the solid model of the target is predefined and projected to 2D images. Then, the relative pose is calculated by comparing the projected solid model image with the captured 2D images by dual cameras.

Left and right cameras are mounted in vehicle in fixed and parallel position. Coordinate frames of image, camera, vehicle and model are defined as shown in **Fig. 2**. Searching area is assumed to be around the target as shown in **Fig. 3**. The relative pose between ROV and 3D marker is determined by six parameters $(x, y, z, \epsilon_1, \epsilon_2, \epsilon_3)$, where the first three are position in Cartesian coordinate frame and the latter are orientation in Euler coordinate system represented by unit quaternion avoiding singularity issues [30].

Figure 4 explains how to estimate the relative pose using 3D model-based matching method. Firstly, 3D marker models with different poses are initially set up in random within searching 3D space. The main task is to find the

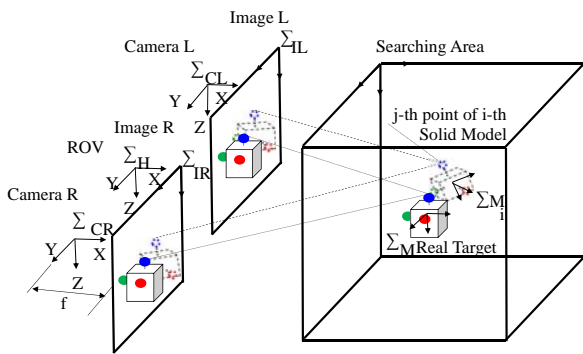


Fig. 2. Model-based pose estimation using dual-eyes vision system.

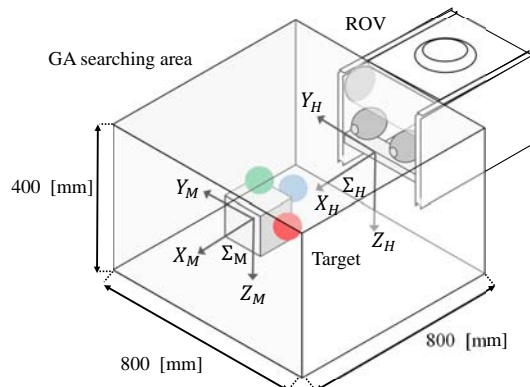


Fig. 3. Coordinate systems and GA search space.

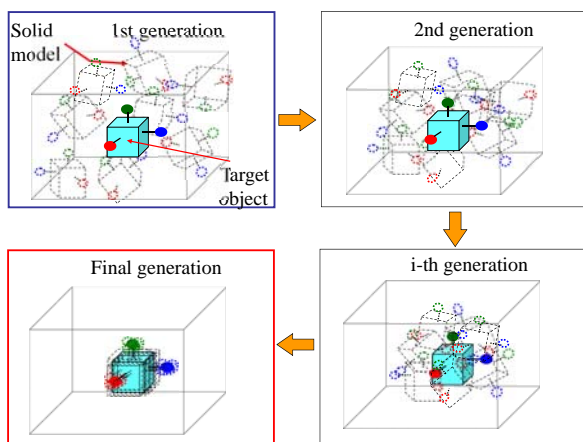


Fig. 4. 3D recognition process.

model that coincides exactly with the real 3D marker and then use the pose of that selected model as the estimated relative pose. To measure the matching degree, we define fitness function to be evaluated in 2D images. However, the number of all possible models within searching area is too huge for system to be evaluated with real-time performance. Therefore, we need optimization method to limit the number of models and generate new models until the best model is detected. In **Fig. 4**, it can be seen that a number of 3D models are initiated in random. Then, they are projected to 2D image planes of left and right cameras and matched with real target images using fitness value.

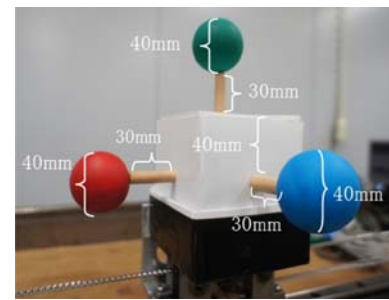


Fig. 5. 3D marker design.

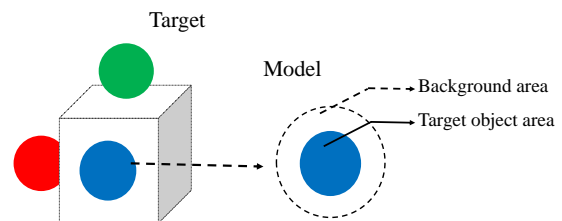


Fig. 6. Target and model object.

Based on some fitter models, new models are generated until generated models approach to the real target. Finally, the best model is detected and the pose of detected model is selected as the estimated one. Note that this recognition process has to be performed within video rate (33 ms in our system).

3.1.1. 3D Marker Design

Target object is designed as shown in **Fig. 5** named as the 3D marker that consists of three spheres (40 mm in diameter) whose colors are red, green and blue. As it is the passive type object, its advantages are simplicity, full information and no power needed. The basic colors are chosen because of their distance to each other in hue value space that is less sensitive to the environment. In some works [10, 11], the target is array of LED light that needs power, image pre-processing such as edge detection against reflection issues. On the other hand, the resolution of the pose especially orientation is limited when the LED source is hidden partially and frequently. Moreover, the concept based on the group of pixels rather than individual pixels in proposed system highlights merits of model-based method over feature-based ones.

3.1.2. Fitness Function

To estimate the relative pose by comparing target object and object models, fitness value that is correlation function representing a matching degree of projected model against the real target in the image is used as the evaluation parameter. As shown in **Fig. 6**, there are two areas in model object to score fitness value namely; the inner one that is the same size as the target sphere and the another one is background area. The portion of the captured target that lies inside the inner area of model will score up the fitness value and the portion that lies inside of the background area will score down the fitness value. It means

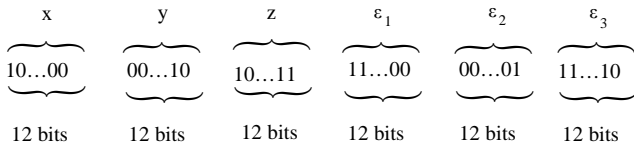


Fig. 7. Gene representing for position and orientation.

the fitness value will be maximum when the target and the model are in coincidence. The overall fitness value is calculated from left image and right image. The detailed explanation can be seen in previous works [31–33].

3.2. 1-Step GA

Left and right images are directly matched with the searching models until one of the models that has the maximum fitness value is found to represent the truthful pose. Consideration of all possible models in searching area is time consuming for real-time application. Therefore, the searching problem addresses to the optimization one. According to the effectiveness, simplicity and repeatable evaluation performance, 1-step GA is used in this experiment. GA named as 1-step GA is capable of real-time recognition of the target object. The effectiveness of 1-step GA was confirmed in robots especially manipulators and reported in previous works [30, 34–37]. The stability of the system was also confirmed by means of Lyapunov analysis in previous work [36]. In this method, the genes as shown in **Fig. 7** that represent the different relative poses of 3D model to the ROV are initiated randomly and evaluated to get the best gene that represents the actual pose of the object. **Fig. 7** shows a gene representing position and orientation with 12 bit per each parameter. Selection of number of bits for each parameter is to get maximum resolution of pose based on the PC performance. Through the steps of GA (Selection, Cross over and Mutation), a number of genes that represent different poses are evaluated by the defined fitness function to get the best gene with the most truthful estimated pose. Property of forwarding the top gene candidates to next generation highlights the robustness of the system against disturbances that may be resulted from image noises even when the target object can be seen partially. The speed of evaluation of gene covers the video rate that is 33 ms so that the genes can be evaluated up to 9 times in the experiments as shown in **Fig. 8**.

3.3. Controller

To eliminate the error in relative pose to the target, conventional P controller is used as shown in Eqs. (1)–(4). Even though the proposed system estimates all six variables of pose, torque around x -axis and y -axis are neglected in control system because the x -axis and y -axis rotations are naturally restored to zero by the restoration torque made by the z -axis distance between the center of buoyance and the one of gravity. Therefore, only four degree of freedom is considered in control system. ON-OFF

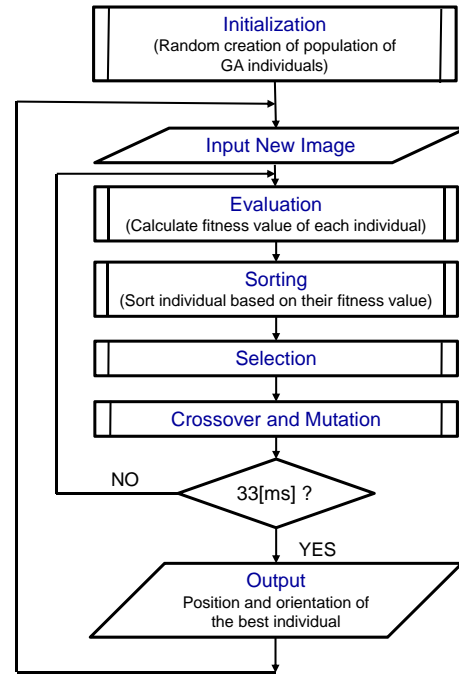


Fig. 8. Flowchart of 1-step GA.

control is used for control in left and right direction (y -axis) and the other three degree of freedom are controlled by P controller. According to the recognition accuracy that is millimeter level and experimental results in movement of ROV, the threshold for ON-OFF control is defined to be 5 mm as shown in Eq. (2). The proportional gain for each thruster is tuned according to the experimental results. The block diagram of the proposed control system is shown in **Fig. 9**.

Back and forth direction : $v_1 = k_{p1}(x_d - x) + 2.5$
 (X_H axis in **Fig. 3**) : $(v_1 = 0 \text{ V for thrust } 9.8 \text{ N in } X_H \text{ of } \Sigma_H, v_1 = 5 \text{ V for } -9.8 \text{ N})$ (1)

Left and right direction : $v_2 = \begin{cases} 5 \text{ V} & ((y_d - y < -5 \text{ mm}) \text{ for thrust in } Y_H \text{ of } \Sigma_H \text{ is } -4.9 \text{ N}) \\ 2.5 \text{ V} & ((-5 \leq y_d - y \leq 5) \text{ meaning thrust equals to zero}) \\ 0 \text{ V} & ((y_d - y > 5 \text{ mm}) \text{ for thrust in } Y_H \text{ of } \Sigma_H \text{ is } 4.9 \text{ N}) \end{cases}$ (2)

Rotation (around Z_H axis in **Fig. 3**) : $v_3 = k_{p2}(\epsilon_{3d} - \epsilon_3) + 2.5$
 ($v_3 = 0 \text{ V for } 0.882 \text{ N in } Z_H \text{ of } \Sigma_H, v_3 = 5 \text{ V for } -0.882 \text{ N})$ (3)

Vertical direction : $v_4 = k_{p3}(z_d - z) + 2.5$
 ($v_4 = 0 \text{ V for } -4.9 \text{ N in } Z_H \text{ of } \Sigma_H, v_4 = 5 \text{ V for } 4.9 \text{ N})$ (4)

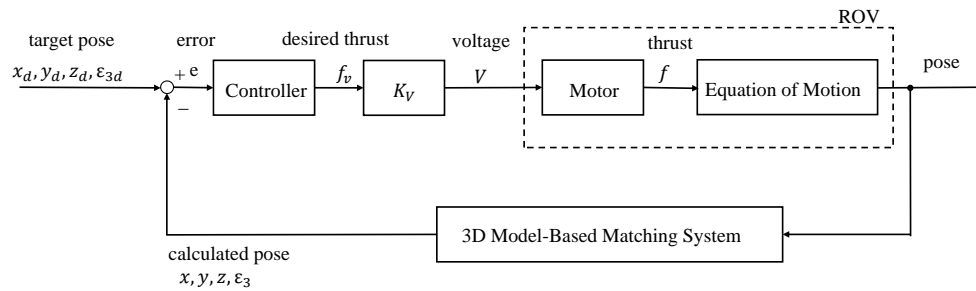


Fig. 9. Control logic for the proposed system.

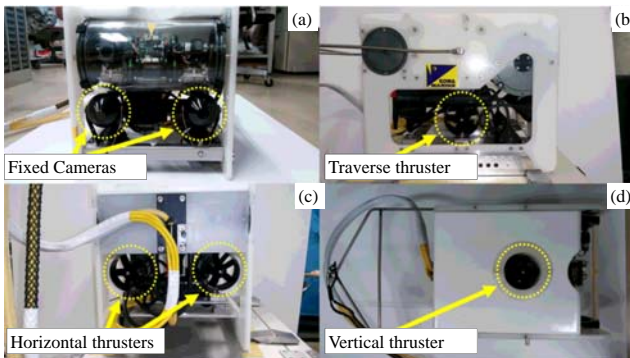


Fig. 10. Overview of ROV: (a) front view, (b) side view, (c) top view, (d) back view.

where, v_1 is input voltage for each of two horizontal thrusters (shown in Fig. 10(c)) for movement of ROV in back and forth direction (X_H in Fig. 3); v_2 is input voltage for traverse thruster (shown in Fig. 10(b)) for movement of ROV in right and left direction (Y_H in Fig. 3); v_3 is input voltage for thrusters for rotation movement of ROV around z -axis (Z_H in Fig. 3), and v_4 is input voltage for vertical thruster (shown in Fig. 10(d)) for movement of ROV in vertical direction (Z_H in Fig. 3). Note that the rotation of vehicle is controlled by two horizontal thrusters that rotate in opposite direction.

3.4. Underwater Vehicle

Remotely controlled underwater robot used in this experiment (manufactured by KOWA, maximum depth 50 m) is shown in Fig. 10. Two fixed forward cameras with the same specification (imaging element CCD, pixel number 380,000 pixel, signal system NTSC, minimum illumination 0.8 lx, no zoom) are mounted on ROV. The two fixed forward cameras are used for three-dimensional object recognition in visual servoing. In the thruster system of ROV, 2 horizontal thrusters with maximum thrust of 9.8 N, 1 vertical thruster with maximum thrust of 4.9 N and 1 traverse thruster with 4.9 N are installed. In addition, it has been equipped with two units of LED lights (5.8 W) for illumination source. The ROV used in this experiment is actuated in 4 degrees of freedom (DoF) (x , y , z and ϵ_3). The specifications of main hardware components are summarized in Table 1.

Table 1. Specification of ROV.

Max: operating depth [m]	50
Dimension [mm]	280 (W) \times 380 (L) \times 310 (H)
Dry weight [kg]	15
Number of thrusters	2 (horizontal), 1 (vertical) 1 (traverse)
Number of cameras	2 (Front, fixed), 2 (Downward, fixed), 1 (tilting and zooming)
Number of LED lights	2 (5.8 W)
Number of line lasers	2 (2 mW)
Tether cable [m]	200
Structural materials	Aluminum alloy and acrylate resin
Maximum thrust force [N]	9.8 (horizontal), 4.9 (vertical, traverse)

4. Experiment of Visual Servoing

Experiments were conducted in simulated environment in order to verify the effectiveness of the proposed visual servoing. Firstly, the experiment in which the underwater robot keeps the relative pose with fixed target, was conducted while setting the experimental conditions approving that the robot is regulated to the final pose against the target object. Secondly, the robustness against the physical disturbance was verified while visual servoing. Finally, the experiments were conducted in the case when the target is seen partially.

4.1. Experimental Environment

A pool (length \times width \times height, 2 m \times 3 m \times 0.75 m) filled with tap water was used as an experimental tank for underwater vehicle experiments. ROV is tethered through an cable with 200 m length to receive image information and control signals as shown in Fig. 11. Based on the images which are given by binocular camera, the 3D information is calculated through model-based matching method and Genetic Algorithm (GA). For physical disturbance to disturb the movement of the vehicle, abrupt external forces are applied to the vehicle by pushing the vehicle in different direction using a rod. In order to perform experiments to confirm the robustness of the system in case when the target is seen partially, one of the three

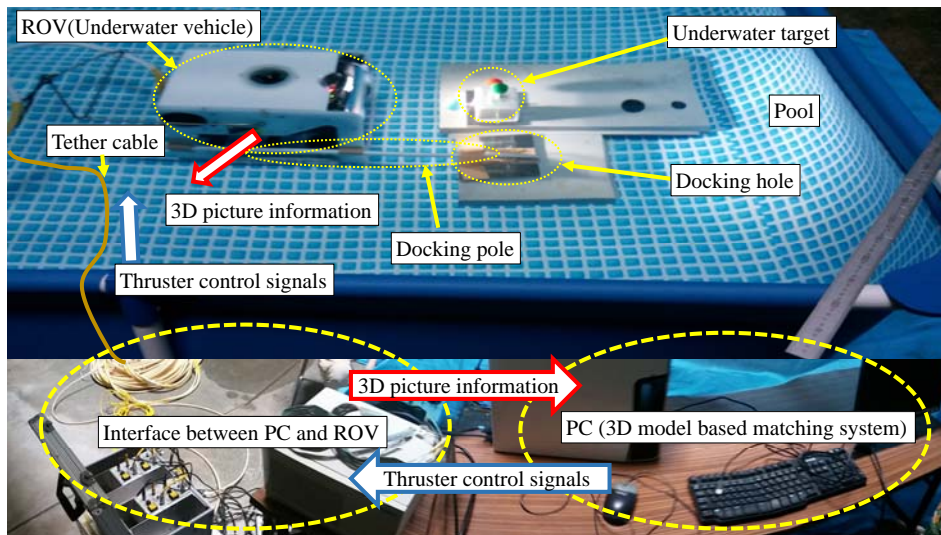


Fig. 11. Layout of underwater experimental devices.

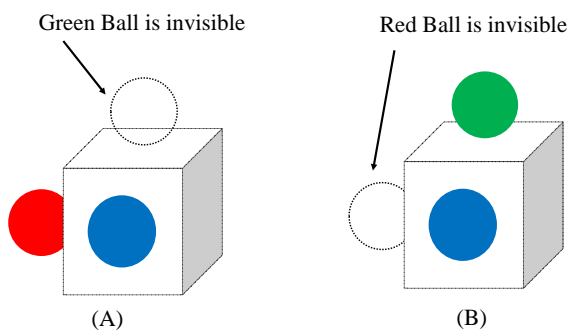


Fig. 12. In the case when target is seen partially: (A) green ball is invisible, (B) red ball is invisible.

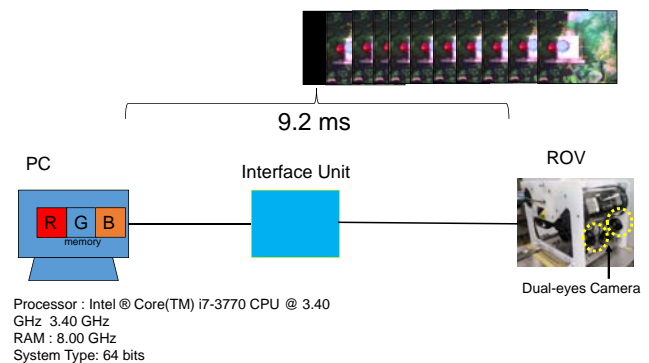


Fig. 13. Interface between robot and PC.

spears is hidden for some times. In Fig. 12(A), the green ball is hidden for few seconds while visual servoing and Fig. 12(B) shows the case when the red ball is invisible.

4.2. System Configuration

4.2.1. Adjustment of Dead Zone

For manual operation by joystick instructions of the controller in the remote-operated ROV, it has to have a certain amount of dead zone voltage that makes thrusters with no thrust in order to prevent malfunction due to the motion of a human finger. On the other hand, in this study, when approaching to the object by thruster propulsion, the realization of the movement as well as the attitude control performance of high accuracy is in millimeter. Therefore, the characteristic of thrust of each thruster that changes with respect to the dead zone in the control voltage can be easily configured by using formulation in thrust approximation. Specifically, the dead band characteristics of the ROV which was confirmed in preliminary experiments are removed by means of linear approximation as a solid line and thrust was configured in the control software so as to generate.

4.2.2. Camera Calibration

Precise calibration is critical factor where the task (pose estimation in this work) to be achieved is expressed in Cartesian space rather than image space. Therefore, camera calibration process utilizing the projective transformation and the epipolar constraints of the baseline stereo (parallel stereo) camera model has been taken carefully along with the experiments.

4.2.3. Interfacing

Figure 13 shows the interfacing between proposed system implemented in PC and the camera mounted in robot. As the resolution of pose is in 12 bits, digital to analog converter with high resolution is used for precise control. Even though there is initial delay time about 9 ms in receiving dynamic video images with 33 ms, it does not come in picture as issues for real-time operation.

4.2.4. Adjustment of Cable Tension

As the experimental environment is indoor pool, there is space limitation for vehicle that is tethered through an

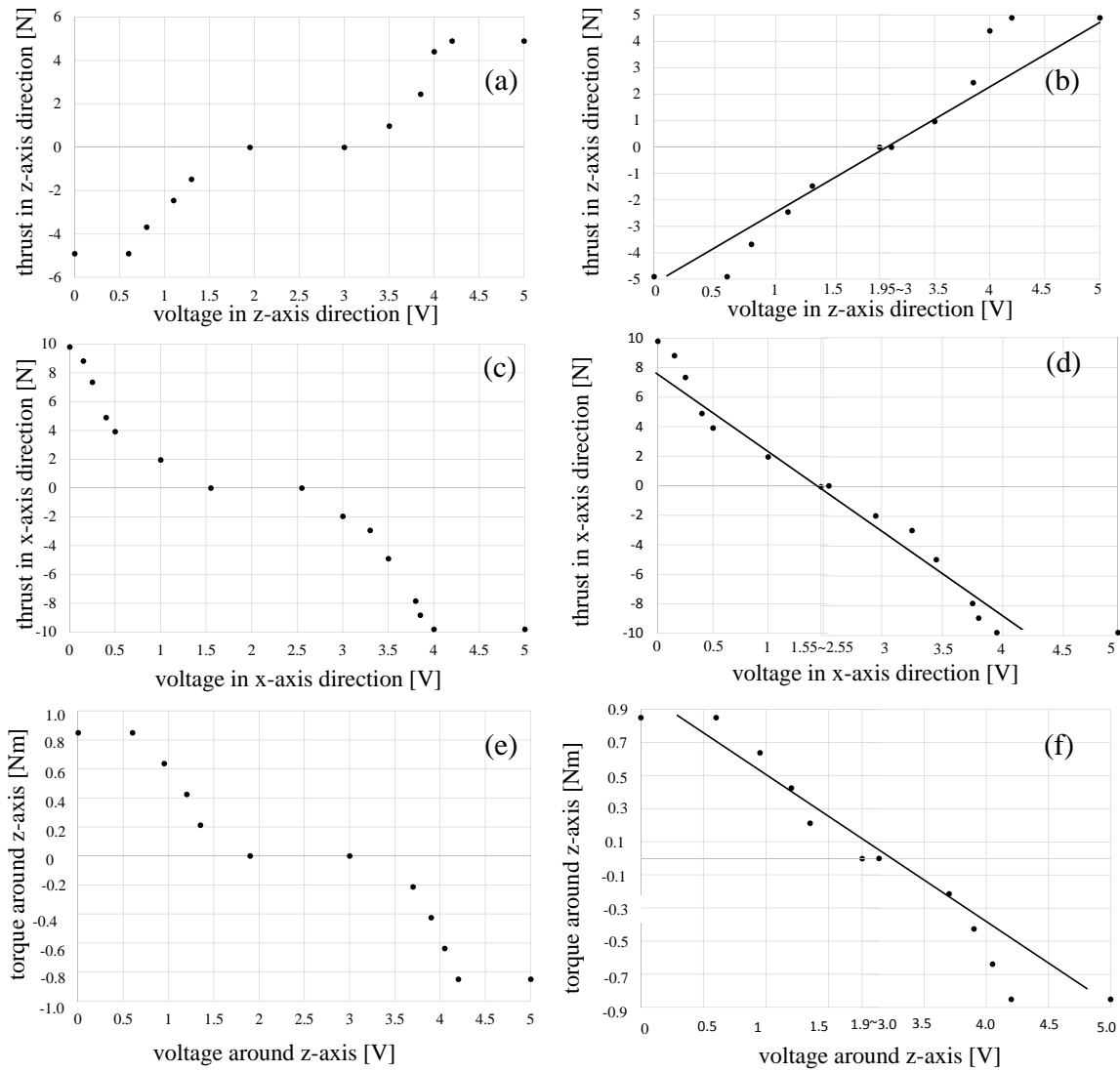


Fig. 14. Initial characteristics of thrust and torque control voltage and adjusted ones by removing dead-band and linearization: (a) initial characteristics in z-axis direction, (b) characteristics removing dead-band (solid line) and adjusted one (black dot) in z-axis direction, (c), (d) characteristics in x-axis direction and (e), (f) characteristics around z-axis.

cable. Therefore, cable tension may cause sometimes disturbance in controlling the vehicle that should be in 4 DoF. However, careful adjustment of cable position eliminates these small issues while conducting experiments.

4.2.5. Desired Pose Setting

According to the range of camera for recognition and experimental environment scale, the desired pose is set as below. The negative distance in z-axis is the difference between the origin of the camera and vehicle frame Σ_H .

$$\begin{aligned} x_d &= {}^H x_M = 600 \text{ mm}, & y_d &= {}^H y_M = 0 \text{ mm}, \\ z_d &= {}^H z_M = -67 \text{ mm}, & \epsilon_{3d} &= 0^\circ \end{aligned}$$

where, x [mm], y [mm], z [mm], ϵ_3 [$^\circ$] represent the position and orientation of the target object recognized by GA. In order to regulate the underwater robot with this desired relative pose to the target, the command voltage

values $v_1 \sim v_4$ fed to respective thrusters are calculated from P controller.

5. Results and Discussion

5.1. Linearization of Dead Zone Voltage in Thrusters

To remove the dead zone in control voltage, the linearization of control voltage is performed according to the experimental adjustment as shown in Fig. 14. Figs. 14(a), (c), (e) show the initial characteristics of thrust and torque control voltage observed in experimental measurements and (b), (d), (f) are their corresponding adjusted ones.

5.2. 3D Recognition Accuracy

Figure 15(a) shows the time variation of the fitness value at the time of GA recognition of underwater robot

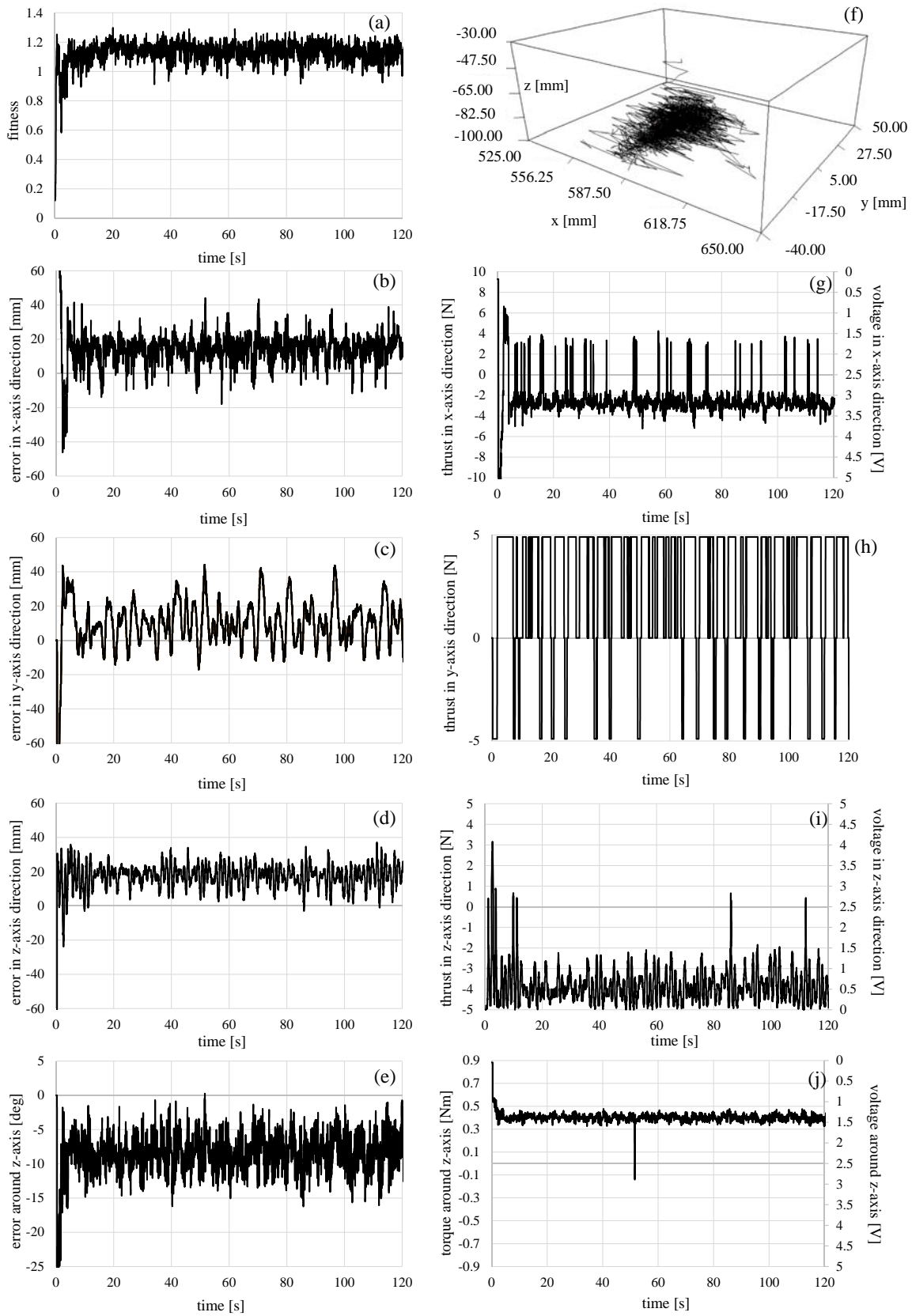


Fig. 15. Regulating performance: (a) fitness value, (b) error in x-axis direction, (c) error in y-axis direction, (d) error in z-axis direction, (e) error around z-axis, (f) 3D trajectory of underwater vehicle, (g) thrust in x-axis direction, (h) thrust in y-axis direction, (i) thrust in z-axis direction and (j) torque around z-axis.

Table 2. Parameters for GA.

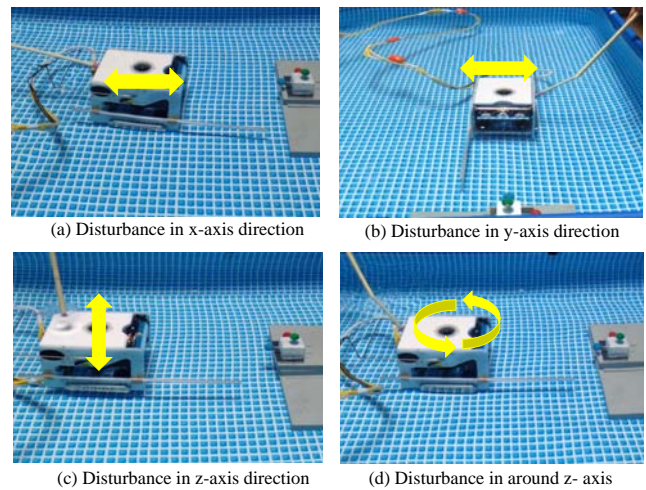
Number of genes	60
Target variables	Positions (x [mm], y [mm], z [mm]), Posture (ϵ_3 [$^\circ$])
Search area [mm]	$\{x, y, z\} = \{\pm 400, \pm 400, \pm 200\}$
Control period [ms]	33
Number of GA evolution	9

that was regulated in $x_d = 600$ mm, $y_d = 0$ mm, $z_d = -67$ mm, $\epsilon_{3d} = 0^\circ$. According to the experiment result, it can be seen that the fitness value is maintained above 0.8 within a few seconds from the recognition start. In general, when performing precise visual servoing, GA recognition accuracy is thought to be necessary 0.5 or more. It was confirmed that the object recognition accuracy in water using GA was almost the same degree of fitness in comparison with the case in the air. This result addresses huge benefit of reducing frequency of doing experiments in water for testing every advanced step in recognition process. Generally, it is difficult to confirm how much speed of moving target can be detected by the speed of evaluation of GA. However, two contributions in the proposed system provide promising performance considering this fact. The first one is that 1-step GA forwards its best candidates to the next generations. On the other hand, the regulating control algorithm keeps field of view of both cameras after initial recognition. For example, when the relative pose makes the invisible of right camera for certain reasons such as the target is moving or the vehicle is physically disturbed after recognition, the control algorithm makes priority to turn left direction while visual servoing. **Table 2** shows the parameters of GA for conducted experiment.

5.3. Regulating Performance

The regulating performance by means of visual servoing is shown in **Fig. 15**. **Fig. 15(a)** shows the fitness value recognized by 1-step GA, **Fig. 15(f)** shows the position of underwater robot in the regulation as measured in 1-step GA and **Figs. 15(b)–(e), (g)–(j)** represent the errors between the relative pose of the target and that of the underwater robot, and the torque to restore it, respectively.

Although error in the relative target pose appears constantly and the four thrusters operate simultaneously, there are some pose fluctuation according to the cable tension during robot movement and reflected waves from the pool sides that occur due to water pressure changes with robot movement. However, the proposed system is able to regulate the relative pose by canceling these disturbance elements. As the lateral thruster control is ON-OFF logic, the position error in this axis may be significant comparing to the others. Therefore, P controller will be adopted for that thruster in near future.

**Fig. 16.** Physical disturbance in different directions: (a) x-axis, (b) y-axis, (c) z-axis, (d) around z-axis.

5.4. Robustness Against Physical Disturbances

The robustness of the proposed system should be verified considering all possibilities that the real environment could provides the vehicle. Therefore, physical disturbances are simulated for proposed system. Abrupt external forces to move the vehicle for distance of 150 ~ 200 mm between 1.5 to 2.0 s in difference directions and to rotate 15° per 1 s for rotation around a vertical axis by means of a rod from the outside of pool are applied as shown in **Fig. 16** and the robustness of the visual servoing is analyzed.

Regulating performance with disturbance in vertical axis is shown in **Fig. 17**. **Fig. 17** shows (a) the fitness of GA recognition, (b) the error between the relative pose of the object target and underwater robot in z-axis direction and, (c) the same results of (b) enlarged view from 55 s to 65 s. The disturbance has been added in each of the figures after 20 s and 60 s from the beginning of the experiment. **Fig. 17(c)** shows enlarged view during regulating response against prodding to be seen how the system behaved in real-time. In the period shown with (A) and (B) in **Fig. 17(d)**, it is found that varying the thrust (torque) is applied to the thrusters in response to error from the relative target pose while maintaining the visual servo although fitness is temporarily lowered when a disturbance is applied. From the above results, the proposed system can be restored to its desired pose within a few seconds ~ several 10 seconds for all of these disturbances. Therefore, it was confirmed that the system is robust against external disturbances.

5.5. Robustness Against Target Visibility

To verify the robustness of the system in terms of target visibility, visual servoing when the object is partially seen was conducted. In simulated environment, one of the spheres was hidden for certain period and the visual servoing performance is analysed. **Fig. 18** shows recognition performance when the red sphere of target object

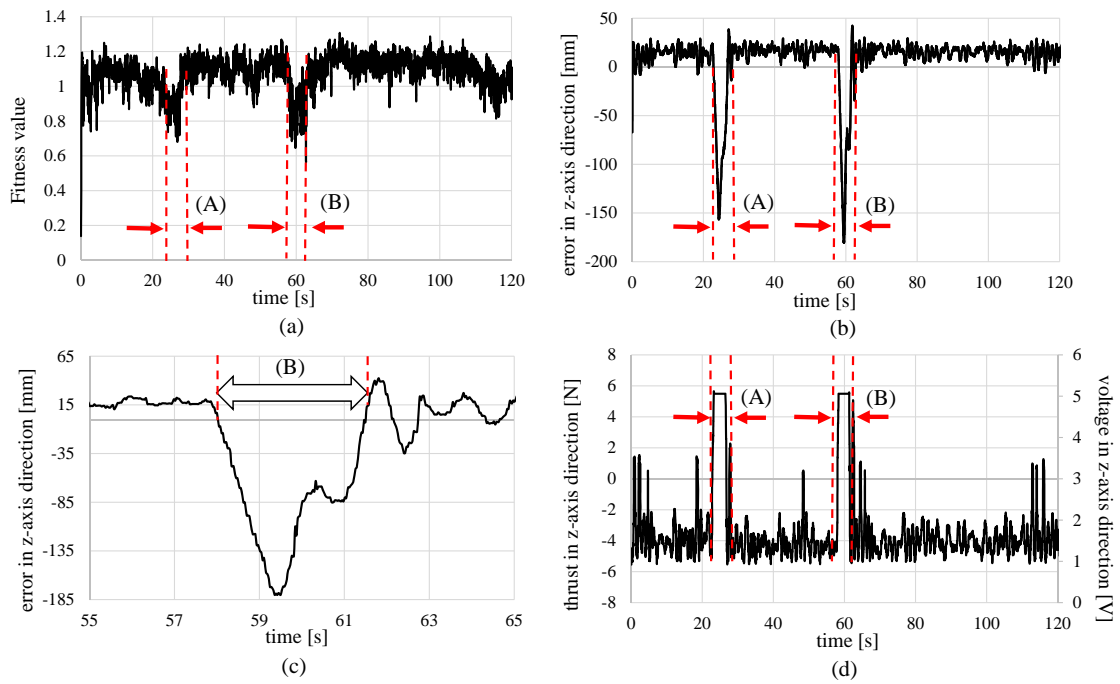


Fig. 17. Regulating performance with disturbance in z-axis direction: (a) fitness value, (b) error in z-axis, (c) error in z-axis (enlarged view from 55 s to 65 s) and (d) torque in z-axis.

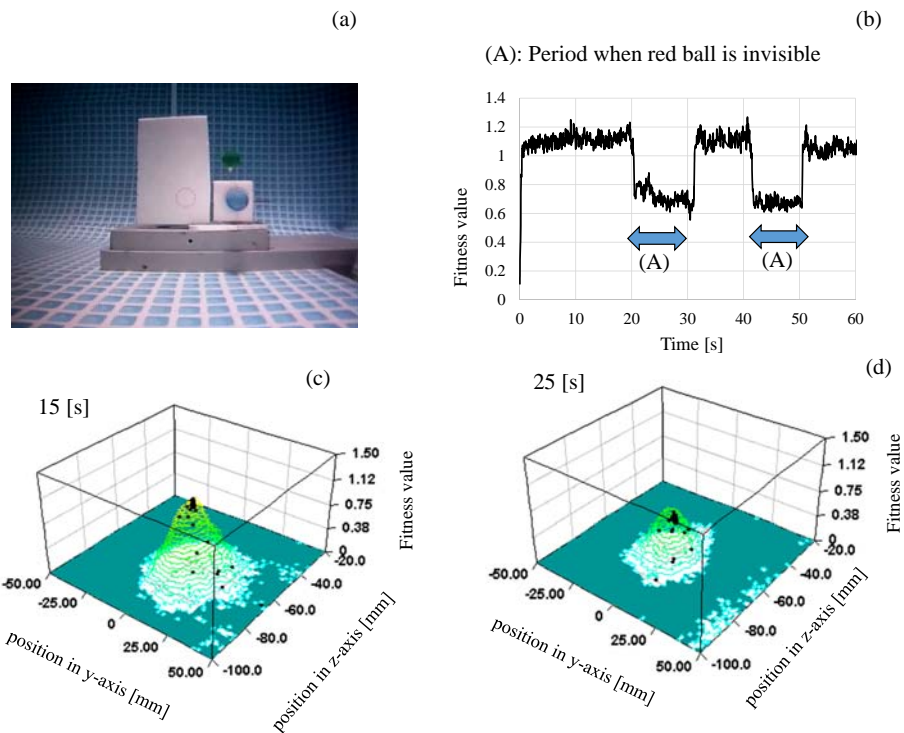


Fig. 18. Recognition performance: (a) recognized model and real target, (b) fitness value when red ball is hidden in some period, (c) comparison of full search and GA search when all three balls are visible, (d) comparison of full search and GA search when red ball is invisible.

is invisible for some period shown as (A), and **Fig. 19** shows the result when green sphere is being hidden from the view of the vehicle’s camera. As shown in figures, the fitness value is reduced for the period when target is partially seen. To evaluate the proposed system utilizing

1-step GA, recognition results are compared to the system in which the best gene is searched throughout all possible poses without using GA. For instance, the recognized positions in z-y plane with respect to fitness are shown in **Figs. 18** and **19**. The poses evaluated in full searching are

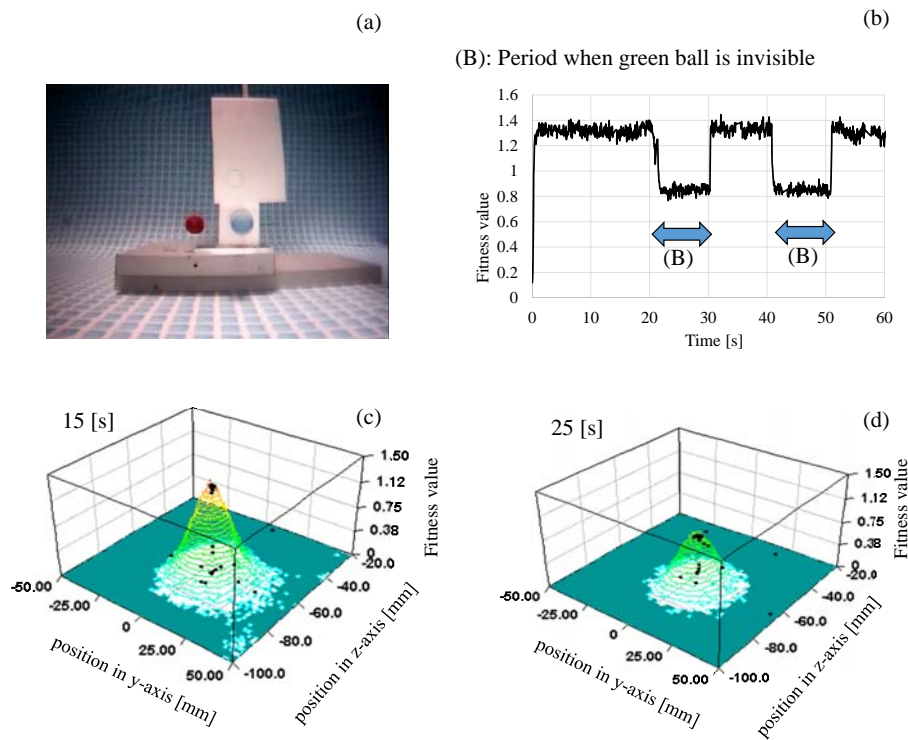


Fig. 19. Recognition performance: (a) recognized model and real target, (b) fitness value when green ball is hidden in some period, (c) comparison of full search and GA search when all three balls are visible, (d) comparison of full search and GA search when green ball is invisible.

represented as contour and the ones evaluated by 1-step GA are shown as black dotted ones. These results highlight the promising optimization performance of GA to find the best gene using only some selected candidates for real-time. **Figs. 20** and **21** are snap photos of conducting the visual servoing when the target object is partially hidden. It can be seen that the system is able to estimate the relative pose even one ball is hidden. The estimated model of the hidden ball can be seen as dotted circle in cover white plane.

Figure 22 shows the regulating performance when the red ball is hidden during 20–30 seconds and 40–50 seconds from the view of the vehicle. Firstly the system recognizes the object with 1.2 fitness value in few seconds. Then, it can be seen that the fitness value reduces to around 0.8 from 1.2 for the period in which the red ball is hidden. According to the experimental results as shown in **Figs. 22(b), (c), (d)**, however, the proposed system can maintain pose estimation accuracy and regulating performance even the object is partially occluded. The position error in y-axis direction is significant comparing to others because of the ON-OFF control in transverse direction thruster. According to the several experiments, it was confirmed that the proposed system is robust not only for physical disturbances but also when the object itself is partially seen. Therefore, the proposed passive 3D marker with known color, size and especially structure, and 1-step GA which forwards the best genes to the next generation might make this robustness come true in picture.

6. Conclusion

For the applications where high homing accuracy are needed, we have developed ROV using proposed visual servoing. In this study, we carried out underwater experiments with regulating performance using visual servoing by dual-eyes cameras. The experimental results show not only high recognition accuracy about ± 20 mm but also real-time application utilizing 3D model-based matching and 1-step GA for optimization in pose estimation. Some experiments were conducted to verify the robustness of the proposed system against physical disturbances in different directions. The system can restore the relative target pose of the object against physical disturbances in visual servoing. Therefore, the proposed system is stable against external force disturbances. Finally, the recognition accuracy and regulating performance are reported in the case when the object is partially seen. These results highlight the effectiveness of the proposed system. As a future plan, sea trial experiments will be conducted in near future.

References:

- [1] F. Chaumette and S. Hutchinson, "Visual servo control I: Basic approaches," *IEEE Robot. Autom. Mag.*, Vol.13, No.4, pp. 82-90, Dec. 2006.
- [2] F. Chaumette and S. Hutchinson, "Visual servo control II: Advanced approaches," *IEEE Robot. Autom. Mag.*, Vol.14, No.1, pp. 109-118, Mar. 2007.
- [3] F. Janabi-Sharifi, L. Deng, and W. J. Wilson, "Comparison of basic visual servoing methods," *IEEE/ASME Trans. on Mechatronics*, Vol.16, No.5, October 2011.

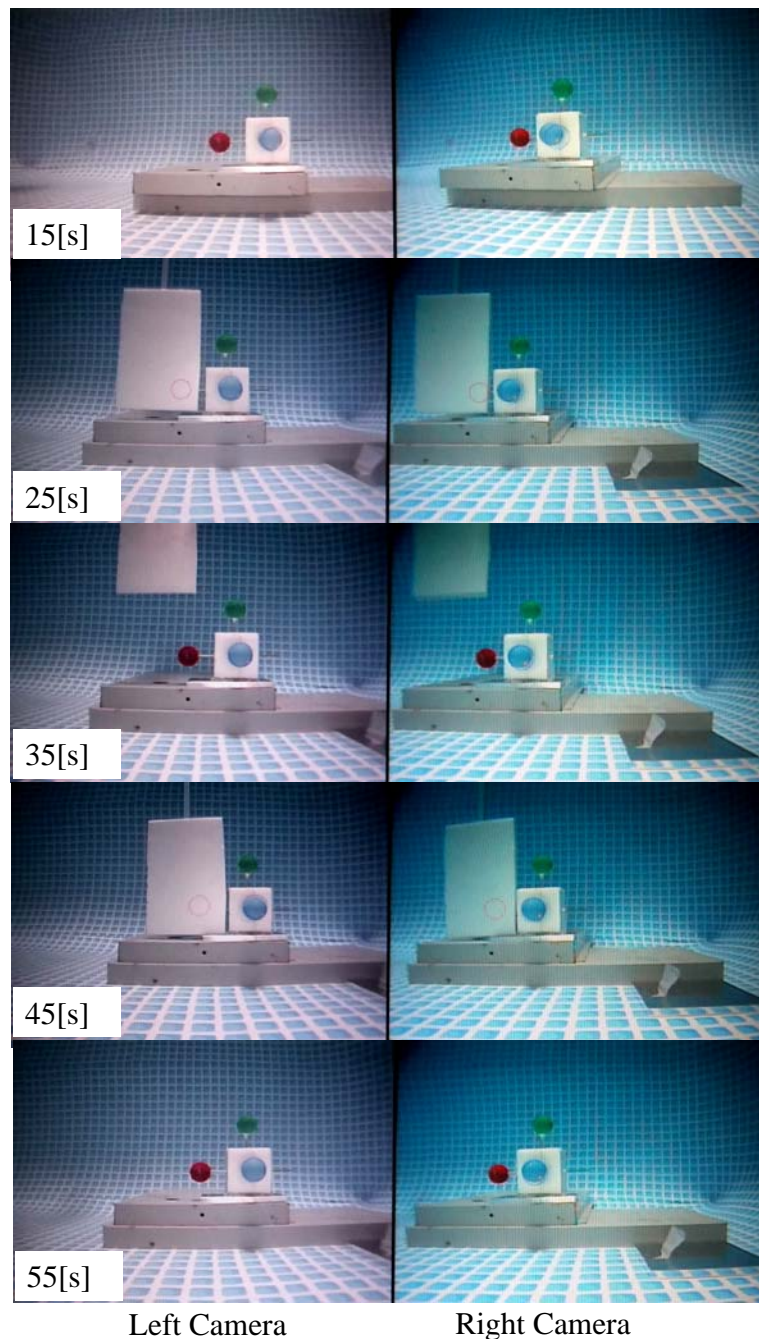


Fig. 20. Left and right camera images when the red ball is invisible between 20 s to 30 s and 40 s to 50 s.

- [4] Y. Okuda, H. Kamada, S. Takahashi, S. Kaneko, K. Kawabata, and F. Takemura, "Method of dynamic image processing for ecology observation of marine life," *J. of Robotics and Mechatronics*, Vol.25, No.5, pp. 820-829, 2013.
- [5] D. Lee, X. Tao, H. Cho, and Y. Cho, "A dual imaging system for flip-chip alignment using visual servoing," *J. of Robotics and Mechatronics*, Vol.18, No.6, pp. 779-786, 2006.
- [6] G. L. Foresti, S. Gentili, and M. Zampato, "A vision-based system for autonomous underwater vehicle navigation," *OCEANS '98 Conf. Proc.* (Vol.1), pp. 195-199, 1998.
- [7] J.-Y. Park, B.-H. Jun, P.-M. Lee, and J. Oh, "Experiments on vision guided docking of an autonomous underwater vehicle using one camera," *Ocean Eng.*, Vol.36, No.1, pp. 48-61, Jan. 2009.
- [8] T. Ura, Y. Kurimoto, H. Kondo, Y. Nose, T. Sakamaki, and Y. Kuroda, "Observation behavior of an AUV for ship wreck investigation," *Proc. of the OCEANS 2005 MTS/IEEE Conf.*, Vol.3, pp. 2686-2691, 2005.
- [9] N. Palomeras, P. Ridao, D. Ribas, and G. Vallicrosa, "Autonomous I-AUV docking for fixed-base manipulation," *Preprints of the Int. Federation of Automatic Control*, pp. 12160-12165, 2014.
- [10] S. Sagara, R. B. Ambar, and F. Takemura, "A stereo vision system for underwater vehicle-manipulator systems – proposal of a novel concept using pan-tilt-slide cameras –," *J. of Robotics and Mechatronics*, Vol.25, No.5, pp. 785-794, 2013.
- [11] Y. Li, Y. Jiang, J. Cao, B. Wang, and Y. Li, "AUV docking experiments based on vision positioning using two cameras," *Ocean Engineering*, Vol.110, pp. 163-173, December 2015.
- [12] F. Maire, D. Prasser, M. Dunbabin, and M. Dawson, "A vision based target detection system for docking of an autonomous underwater vehicle," *Australasian Conf. on Robotics and Automation (ACRA)*, Sydney, Australia, December 2-4, 2009.
- [13] S. Ishibashi, "The stereo vision system for an underwater vehicle," *Oceans 2009, Europe, Bremen*, pp. 1343-1348, 2009.
- [14] S. Cowen, S. Briest, and J. Dombrowski, "Underwater docking

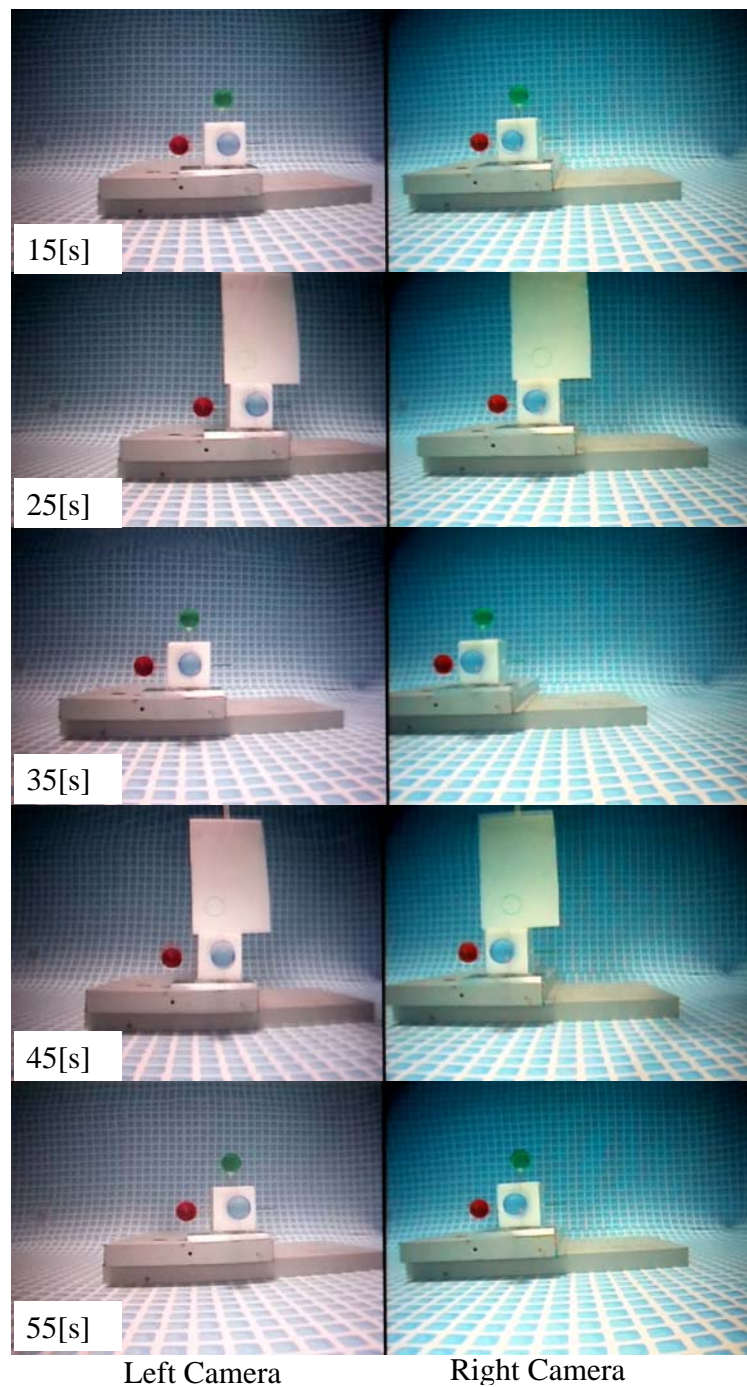


Fig. 21. Left and right camera images when the green ball is invisible between 20 s to 30 s and 40 s to 50 s.

of autonomous undersea vehicle using optical terminal guidance," Proc. IEEE Oceans Engineering, Vol.2, pp. 1143-1147, 1997.

- [15] K. Teo, B. Goh, and O. K. Chai, "Fuzzy docking guidance using augmented navigation system on an AUV," IEEE J. of Oceans Engineering, Vol.37, No.2, April 2015.
- [16] M. D. Feezor, F. Y. Sorrell, P. R. Blankinship, and J. G. Bellingham, "Autonomous underwater vehicle homing/docking via electromagnetic guidance," IEEE J. of Oceans Engineering, Vol.26, No.4, pp. 515-521, October 2001.
- [17] R. S. McEwen, B. W. Hobson, L. McBride, and J. G. Bellingham, "Docking Control System for a 54-cm-Diameter (21-in) AUV," IEEE J. of Oceanic Engineering, Vol.33, No.4, pp. 550-562, October 2008.
- [18] K. Teo, E. An, and P.-P. J. Beaujean, "A robust fuzzy autonomous underwater vehicle (AUV) docking approach for unknown current disturbances," IEEE J. of Oceanic Engineering, Vol.37, No.2, pp. 143-155, April 2012.
- [19] J.-Y. Park, B.-H. Jun, P.-M. Lee, F.-Y. Lee, and J.-h. Oh, "Experiment on underwater docking of an autonomous underwater vehicle 'ISiMI' using optical terminal guidance," IEEE Oceanic Engineering, Europe, pp. 1-6, 2007.
- [20] A. Negre, C. Pradalier, and M. Dunbabin, "Robust vision-based underwater homing using self similar landmarks," J. of Field Robotics, Wiley-Blackwell, Special Issue on Field and Service Robotics, Vol.25, No.6-7, pp. 360-377, 2008.
- [21] M. Dunbabin, B. Lang, and B. Wood, "Vision-based docking using an autonomous surface vehicle," IEEE Int. Conf. on Robotics and Automation, Pasadena, CA, USA, 2008.
- [22] P. Batista, C. Silvestre, and P. Oliveira, "A two-step control strategy for docking of autonomous underwater vehicles," American Control Conf., Fairmont Queen Elizabeth, Montréal, Canada, 2012.

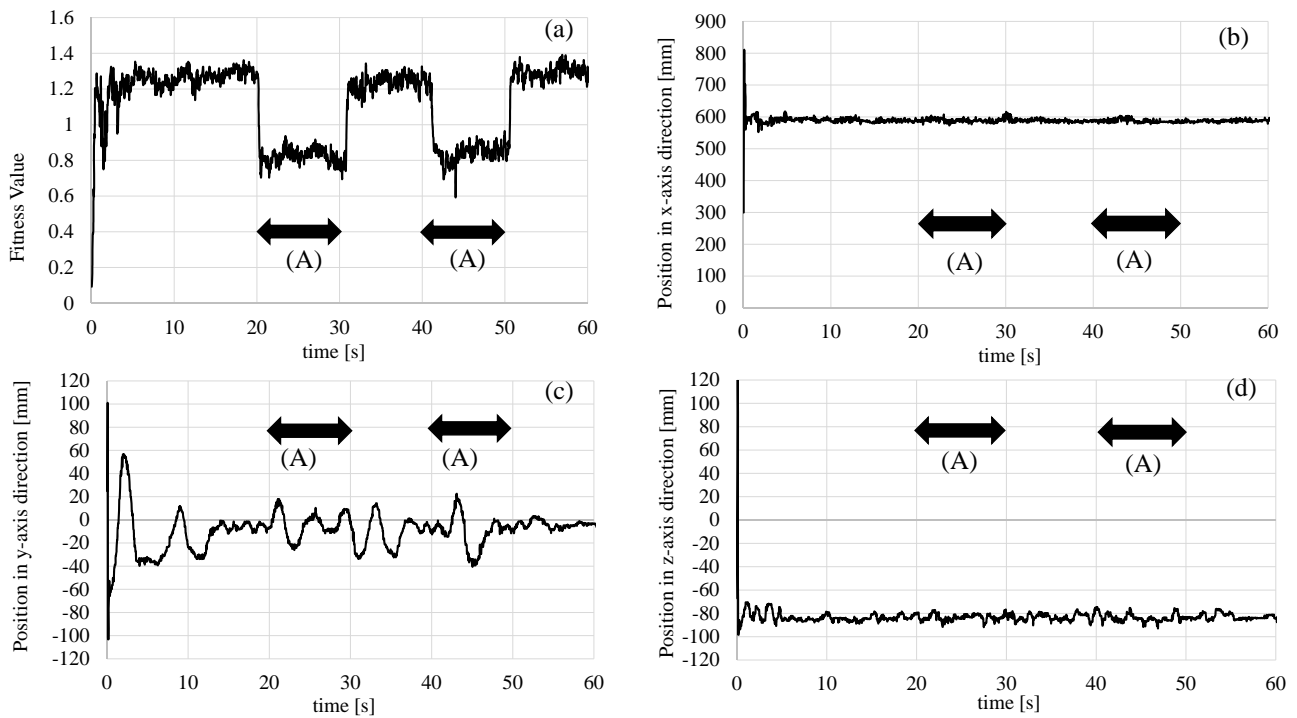


Fig. 22. Regulating performance when the object is partially seen: (a) fitness value, (b) position in x -axis direction, (c) position in y -axis direction, (d) position in z -axis direction.

- [23] N. Palomeras, A. Peñalver, M. Massot-Campos, G. Vallicrosa, P. L. Negre, J. J. Fernández, P. Ridaó, P. J. Sanz, G. Oliver-Codina, and A. Palomer, "I-AUV docking and intervention in a subsea panel," *IEEE/RSJ Int. Conf. on Intelligent Robots and Systems*, Chicago, IL, pp. 2279-2285, 2014.
- [24] S.-C. Yu, T. Ura, T. Fujii, and H. Kondo, "Navigation of autonomous underwater vehicles based on artificial underwater landmarks," *OCEANS MTS/IEEE Conf. and Exhibition*, Vol.1, pp. 409-416, 2001.
- [25] L. Vacchetti and V. Lepetit, "Stable real-time 3D tracking using on-line and offline information," *Trans. on Pattern Analysis and machine Intelligence*, Vol.26, No.10, pp. 1385-1391, 2004.
- [26] C. Choi, S.-M. Baek, and S. Lee, "Real-time 3D object pose estimation and tracking for natural landmark based visual servo," *IEEE/RSJ Int. Conf. on Intelligent Robots and Systems*, pp. 3983-3989, 2008.
- [27] N. P. Papanikolopoulos, P. K. Khosla, and T. Kanade, "Visual tracking of a moving target by a camera mounted on a robot: a combination of control and vision," *IEEE Trans. on Robotics and Automation*, Vol.9, No.1, pp. 14-35, Feb. 1993.
- [28] G. Panin and A. Knoll, "Fully automatic real-time 3D object tracking using active contour and appearance models," *J. of Multimedia*, Vol.1, No.7, pp. 62-70, 2006.
- [29] H. Hajimolhoseini, R. Amirfattahi, and S. Khorshidi, "Real-time pose estimation and tracking of rigid objects in 3D space using extended Kalman filter," *22nd Iranian Conf. on Electrical Engineering (ICEE)*, pp. 1545-1549, 2014.
- [30] W. Song, M. Minami, and S. Aoyagi, "Feedforward on-line pose evolutionary recognition based on quaternion," *J. of the Robot Society of Japan*, Vol.28, No.1, pp. 55-64, 2010 (in Japanese).
- [31] W. Song and M. Minami, "On-line motion-feedforward pose recognition invariant for dynamic hand-eye motion," *IEEE/ASME Int. Conf. on Advanced Intelligent Mechatronics*, pp. 1047-1052, 2008.
- [32] W. Song and M. Minami, "Stability/precision improvement of 6-DoF visual servoing by motion feedforward compensation and experimental evaluation," *IEEE Int. Conf. on Robotics and Automation*, pp. 722-729, 2009.
- [33] W. Song and M. Minami, "Hand and eye-vergence dual visual servoing to enhance observability and stability," *IEEE Int. Conf. on Robotics and Automation*, pp. 714-721, 2009.
- [34] W. Song and M. Minami, "3-D visual servoing using feedforward evolutionary recognition," *J. of the Robot Society of Japan*, Vol.28, No.5, pp. 591-598, 2010 (in Japanese).
- [35] F. Yu, M. Minami, W. Song, J. Zhu, and A. Yanou, "On-line head pose estimation with binocular hand-eye robot based on evolutionary model-based matching," *J. of Computer and Information Technology*, Vol.2, No.1, pp. 43-54, 2012.
- [36] W. Song, M. Minami, F. Yu, Y. Zhang, and A. Yanou, "3-D hand and eye-vergence approaching visual servoing with Lyapunov-stable pose tracking," *IEEE Int. Conf. on Robotics and Automation (ICRA)*, pp. 5210-5217, 2011.
- [37] H. Suzuki and M. Minami, "Visual servoing to catch fish using global/local GA search," *IEEE/ASME Trans. on Mechatronics*, Vol.10, Issue 3, pp. 352-357, 2005.



Name:
Myo Myint

Affiliation:
Okayama University

Address:

3-1-1 Tsushimanaka, Kita-ku, Okayama 700-8530, Japan

Brief Biographical History:

2004- Assistant Lecturer, Electronic Engineering Department, Mandalay Technological University

2008- Lecturer, Electronic Engineering Department, Mandalay Technological University

2011- Assistance Professor, Electronic Engineering Department, Yangon Technological University

Main Works:

- "Robustness of visual-servo against air bubble disturbance of underwater vehicle system using three-dimensional marker and dual-eye cameras," Proc. of the OCEANS 2015 MTS/IEEE Conf. (Washington DC, USA), pp. 1-8, Oct. 20-22, 2015.
- "Visual-servo-based autonomous docking system for underwater vehicle using dual-eyes camera 3D-pose tracking," Proc. of 2015 IEEE/SICE Int. Symposium on System Integration (SII), Nagoya, Japan, pp. 989-994, 2015.

Membership in Academic Societies:

- The Institute of Electrical and Electronics Engineers (IEEE)



Name:
Akira Yanou

Affiliation:
Kawasaki College of Allied Health Professions

Address:

316 Matsushima, Kurashiki, Okayama 701-0194, Japan

Brief Biographical History:

2001 Received Ph.D. in Engineering from Okayama University

2002- Assistant Professor, Faculty of Engineering, Kinki University

2004- Lecturer, Faculty of Engineering, Kinki University

2009- Assistant Professor, Graduate School of Natural Science and Technology, Okayama University

2016- Associate Professor, Department of Radiological Technology, Kawasaki College of Allied Health Professions

Main Works:

- "Autonomous docking control of visual-servo type underwater vehicle system aiming at underwater automatic charging," Trans. of the JSME, Vol.81, No.832, 15-00391, Dec. 2015 (in Japanese).

Membership in Academic Societies:

- The Institute of Electrical and Electronics Engineers (IEEE)
- The Japanese Society of Mechanical Engineers (JSME)
- The Society of Instrument and Control Engineers (SICE)
- The Institute of Systems, Control and Information Engineers (ISCIE)
- Japanese Society of Radiological Technology (JSRT)



Name:
Kenta Yonemori

Affiliation:
Okayama University

Address:

3-1-1 Tsushimanaka, Kita-ku, Okayama 700-8530, Japan

Brief Biographical History:

2015 Graduated from School of Natural Science and Technology, Okayama University

Main Works:

- "Docking control of underwater vehicle system for autonomous underwater automatic charging," Proc. of RSJ2015, 2015.

Membership in Academic Societies:

- The Robotics Society of Japan (RSJ)



Name:
Khin Nwe Lwin

Affiliation:
Okayama University

Address:

3-1-1 Tsushimanaka, Kita-ku, Okayama 700-8530, Japan

Brief Biographical History:

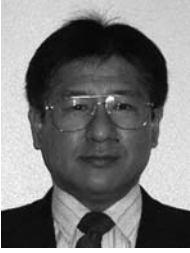
2007- Assistant Lecturer, Mechatronic Engineering Department, Technological University (Monywa)

2009- Assistant Lecturer, Mechatronic Engineering Department, Mandalay Technological University

2012- Lecturer, Faculty of Precision Engineering, University of Technology (Yatanarpon Cyber City)

Main Works:

- performance analysis of multi-step GA for real-time 3D model-based recognition for underwater vehicle



Name:
Mamoru Minami

Affiliation:
Professor, Graduate School of Natural Science
and Technology, Okayama University

Address:
3-1-1 Tsushimanaka, Kita-ku, Okayama 700-8530, Japan

Brief Biographical History:
1990- Doctoral Course Student, Graduate School of Natural Science and
Technology, Kanazawa University
1994- Associate Professor, Department of Mechanical Engineering,
University of Fukui
2002- Professor, Department of Human and Artificial Intelligence
Systems, University of Fukui
2010- Professor, Graduate School of Natural Science and Technology,
Okayama University

Main Works:

- “Reconfiguration Manipulability Analyses for Redundant Robots,”
Trans. of the ASME, J. of Mechanisms and Robotics, Vol.5, No.4,
pp. 1-16, 2013.
- “Visual Servoing to catch fish Using Global/local GA Search,”
IEEE/ASME Trans. on Mechatronics, Vol.10, No.3, pp. 352-357, 2005.

Membership in Academic Societies:

- The Institute of Electrical and Electronics Engineers (IEEE)
- The Japanese Society of Mechanical Engineers (JSME)
- The Society of Instrument and Control Engineers (SICE)
- The Robotics Society of Japan (RSJ)



Name:
Shintaro Ishiyama

Affiliation:
Professor, Graduate School of Science and Engi-
neering, Hirosaki University

Address:
3 Bunkyocho, Hirosaki, Aomori 036-8561, Japan

Brief Biographical History:
1979 Graduated from Tokyo Institute of Technology
1981- Japan Atomic Energy Agency
1990 Received Doctor degree of Engineering from Tokyo Institute of
Technology
2016- Professor, Hirosaki University

Main Works:

- “In-situ vacuum deposition technique of lithium on neutron production
target for BNCT,” Nuclear Inst. and Methods in Physics Research B,
Vol.288, pp. 18-22, 2012.
- “Synthesis of lithium nitride for neutron production target of BNCT by
in situ lithium deposition and ion implantation,” Nuclear Inst. and
Methods in Physics Research B, Vol.293, pp. 42-47, 2012.

Membership in Academic Societies:

- Atomic Energy Society of Japan
- The Japanese Society of Mechanical Engineers (JSME)
- The Institute of Electrical and Electronics Engineers (IEEE)
- The Society of Instrument and Control Engineers (SICE)
